Photoinduced Electron Transfer at Liquid/Liquid Interfaces. Part VI. On the Thermodynamic Driving Force Dependence of the Phenomenological Electron-Transfer Rate Constant

ARTICLE *in* THE JOURNAL OF PHYSICAL CHEMISTRY B · APRIL 2002

Impact Factor: 3.3 · DOI: 10.1021/jp015533o · Source: OAI

3 AUTHORS, INCLUDING:

David J. Fermín
University of Bristol
109 PUBLICATIONS **1,820** CITATIONS
SEE PROFILE

Hubert H Girault
École Polytechnique Fédérale de Lausanne
556 PUBLICATIONS **13,787** CITATIONS
SEE PROFILE

Photoinduced Electron Transfer at Liquid/Liquid Interfaces. Part VI. On the Thermodynamic Driving Force Dependence of the Phenomenological Electron-Transfer Rate Constant

Nicolas Eugster, David J. Fermín,* and Hubert H. Girault

Laboratoire d'Electrochimie, Département de Chimie, Ecole Polytechnique Fédérale de Lausanne, CH-1015 Lausanne, Switzerland

Received: August 31, 2001; In Final Form: December 6, 2001

The dynamics of photoinduced heterogeneous electron transfer between a series of ferrocene derivatives and the heterodimer zinc *meso*-tetrakis(*p*-sulfonatophenyl)-porphyrin ($ZnTPPS^{4-}$) and zinc *meso*-tetrakis(*N*-methylpyridyl)porphyrin ($ZnTMPyP^{4+}$) were studied at the polarized water/1,2-dichloroethane interface. The photocurrent responses originating from the heterogeneous quenching of the heterodimer showed a well-defined dependence on the formal Gibbs energy of electron transfer (ΔG_{et}°). The use of various ferrocene derivatives with different redox potentials and potentiostatic control over the Galvani potential difference across the interface allowed modifying $\Delta G_{et}^{\circ\prime}$ over a range of 1 eV. The photocurrent as a function of $\Delta G_{et}^{\circ\prime}$ can be unambiguously described in terms of a Marcus-type behavior of the phenomenological bimolecular electron-transfer rate constant (k_{et}^{II}). The solvent reorganization energy was estimated to be 1.05 eV, from which an average distance of 0.8 nm between the redox species can be evaluated within the framework of the Marcus model for sharp liquid/liquid boundary. These studies also provided an estimate of the activation-less limit of k_{et}^{II} of 3×10^{-19} cm^4 s^{-1}, which reflects a rather nonadiabatic behaviour of the charge-transfer process. The origin of this nonadiabaticity is connected to the average distance separating the redox species across the interface. Finally, the implications of the observed potential dependence of k_{et}^{II} on current debates about structure and potential distribution across the interface are briefly highlighted.

1. Introduction

Renewed interest on the dynamics of heterogeneous electron transfer across interfaces between two immiscible electrolyte solutions (ITIES) has been driven by recent developments based on scanning electrochemical microscopy (SECM), spectroscopic, and photoelectrochemical techniques.[1,2] One of the most controversial issues is the dependence of the electron-transfer rate constant on the Galvani potential difference across the interface. The potential dependence is determined by the overlap between the concentration profiles of the redox species and the potential distribution across the liquid/liquid boundary. Molecular dynamic simulations,[3,4] neutron reflectivity,[5] and ellipsometry[6] suggest that the solvent density profile can extend in a region on the order of 1 nm. On the other hand, simulations of the ionic distribution based on lattice-gas modeling[7−10] indicate that the Debye lengths associated with the diffuse layers are on the order of 10 nm. Assuming that the distance separating the redox species is determined by the solvent density profiles, it is expected that changes in the Galvani potential difference would have very little effect on the Gibbs energy of electron transfer.

Contrary to the theoretical analyses, experimental studies based on SECM have shown that the bimolecular electron-transfer (k_{et}^{II}) rate constant does exhibit a dependence on the Galvani potential difference.[11−15] These techniques are performed at ideally nonpolarizable interfaces, where the Galvani potential difference is controlled by the concentration ratio of a common ion. The behavior commonly observed can be described in terms of the Butler−Volmer expression. However, few reports based on SECM and steady-state voltammetry on thin electrolyte layers appear to show potential-independent electron-transfer rate constants.[16−19] The deviations from the Butler−Volmer behavior have been rationalized in terms of concentration polarization phenomena, although no quantitative analysis of potential distribution and concentration profile of the ionic redox species has been presented. In a previous study employing ideally polarizable junctions, we have shown that knowledge of the Galvani potential difference allows estimating the effect of concentration polarization and the effective dependence of the electron-transfer rate constant on the Galvani potential difference.[20]

Tuning the standard redox potential of the species at the interface can also change the driving force for electron transfer. This feature opens up the possibility of performing kinetic studies under large formal Gibbs energy of electron transfer (ΔG_{et}°). Indeed, Bard and co-workers have provided evidence of the inverted Marcus region by a combined electrochemiluminescence−SECM approach.[21] However, analysis of the bimolecular rate constant as a function of the overall driving force in terms of the Marcus expression remains a highly controversial issue. In recent studies, the disparate and scattered nature of the results prevents any reliable attempt to estimate either the reorganization energy or the activation-less limit of the rate constant.[19,22,23]

In the present paper, we shall describe a well-defined dependence of the bimolecular electron-transfer rate constant on the driving force over a range of 1 eV at the externally biased water/1,2-dicholoroethane interface. The rate constant is estimated from the photocurrent responses arising from the heterogeneous quenching of water-soluble porphyrins by a group of ferrocene derivatives as a function of the applied Galvani

10.1021/jp015533o CCC: $22.00
Published on Web 03/08/2002

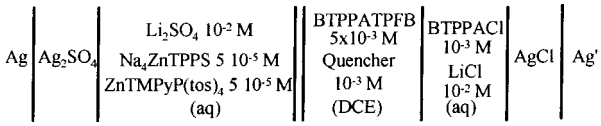

Figure 1. Schematic representation of the electrochemical cell employed for all measurements.

potential difference. The porphyrin employed is the heterodimer formed by zinc *meso*-tetrakis(*p*-sulfonatophenyl)-porphyrin ($ZnTPPS^{4-}$) and zinc *meso*-tetrakis(*N*-methylpyridyl)porphyrin ($ZnTMPyP^{4+}$).[24,25] Previous photoelectrochemical studies have shown that this heterodimer is specifically adsorbed at the liquid/liquid boundary.[26] It was also observed that the photocurrent dependence on the porphyrins' concentration was unaffected by the Galvani potential difference between the two electrolyte phases. This result indicates that the surface coverage of heterodimer is potential-independent; therefore, variations of the photocurrent with the applied potential can be directly related to changes in the kinetics of the electron-transfer process.

2. Experimental Section

2.1. Photoelectrochemical Cell. All reagents employed were analytical grade. The porphyrin salts $(Na)_4ZnTPPS$ and ZnTMPyP(Tosylate)$_4$ were purchased from Porphyrin Products, Inc. Bis(triphenyl-phosphoranylidene) ammonium tetrakis(pentafluorophenyl) borate (BTPPATPFB) and Li_2SO_4 were employed as the organic and aqueous phase-supporting electrolyte, respectively. The preparation of BTPPATPFB has been reported elsewhere.[27]

Measurements were carried out in a three-compartment glass cell provided with two platinum counter electrodes and two luggin capillaries for the reference electrodes. The geometrical surface area was 1.53 cm^2. The electrochemical cell is represented in Figure 1. The water/1,2-dichloroethane (DCE) junction was polarized via a custom-built four-electrode potentiostat, and the potential scale was corrected by the formal transfer potential of the cation tetramethylammonium ($\Delta_o^w \phi^{o\prime}_{TMA^+} = 0.160$ mV).[28] Illumination at 477 nm was provided by a Omnichrome S43 tuneable Ar-ion laser or a 450 W xenon arc lamp (Applied Photophysics).

2.2. Formal Redox Potential of the Porphyrin Excited State and Ferrocene Derivatives. The redox potentials of the ferrocene derivatives employed in this report were estimated following the thermodynamic approach recently highlighted.[1] The formal potential of ferrocene (Fc) in DCE vs SHE, $[E^{o\prime,o}_{Fc^+/Fc}]_{SHE}$, corresponds to the cell reaction

$$^1/_2H_{2(w)} + Fc^+_{(DCE)} \rightarrow H^+_{(w)} + Fc_{(DCE)} \quad (1)$$

To estimate $[E^{o\prime,o}_{Fc^+/Fc}]_{SHE}$, the following thermodynamic cycle can be employed:

$$Fc_{(DCE)}{}^+ \rightarrow Fc^+_{(w)} \quad (2)$$

$$^1/_2H_{2(w)} + Fc^+_{(w)} \rightarrow H^+_{(w)} + Fc_{(w)} \quad (3)$$

$$Fc_{(w)} \rightarrow Fc_{(DCE)} \quad (4)$$

From eqs 1−4, it follows that

$$[E^{o\prime,o}_{Fc^+/Fc}]_{SHE} = \Delta_o^w \phi^{o\prime}_{Fc^+} + [E^{o\prime,w}_{Fc^+/Fc}]_{SHE} - \Delta G^{w\rightarrow o}_{Fc}/F \quad (5)$$

Previous estimations of the parameters in eq 5 for Fc at the water/DCE interface provide a value of $[E^{o\prime,DCE}_{Fc^+/Fc}]_{SHE} = 0.64 \pm 0.02$ V.[1] We shall employ this value as a reference potential for the redox species in the same medium. The formal redox potentials of the ferrocene species were obtained from cyclic voltammetry in DCE on a 25 μm diameter Pt microelectrode at 5 mV s^{-1}. In all cases, the voltammetric responses described a well-defined sigmoidal curve.

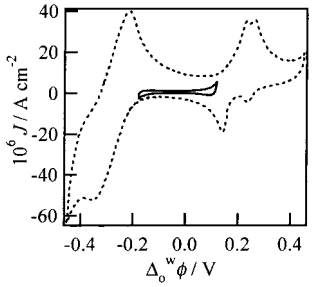

Figure 2. Cyclic voltammograms of the water/DCE interface in the presence of the porphyrin heterodimer in the dark. The composition of the electrolyte solutions is as indicated in Figure 1. The voltammograms were recorded at 0.05 V s^{-1} in the absence of redox quencher. The solid line illustrates the polarizable window employed for the photocurrent studies.

TABLE 1: Formal Redox Potential of the Various Ferrocene Derivatives in 1,2-Dichloroethane and Porphyrin Heterodimer Triplet State vs the Standard Hydrogen Electrode

redox couple	$E^{o\prime}$, V
ferrocene Fc^+/Fc	0.64
dimethylferrocene Me_2Fc^+/Me_2Fc	0.55
diferrocenylethane Fc_2Et^+/Fc_2Et	0.55
butylferrocene $BuFc^+/BuFc$	0.56
decamethylferrocene $Me_{10}Fc^+/Me_{10}Fc$	0.07
^{T}[ZnTPPS/ZnTMPyP] S^-/S^*	1.00

The redox potential of the excited state of the porphyrin heterodimer was estimated from the ground-state redox potential and the energy level of the thermally equilibrated triplet state. A reduction potential for the heterodimer of −0.60 V vs SHE was measured on a hanging mercury electrode (HME). Taking into account that the triplet-state transition for both porphyrins is approximately 1.60 eV,[29,30] the reduction potential of the heterodimer corresponds to 1.0 V. Table 1 summarizes the formal redox potential for the porphyrin excited state as well as the various ferrocene derivatives.

3. Results and Discussion

3.1. Photocurrent Responses at the Porphyrin-Sensitized Water/DCE Interface. The voltammetric behavior of the water/DCE interface in the presence of $ZnTMPyP^{4+}$ and $ZnTPPS^{4-}$ is illustrated in Figure 2. The response observed at negative potentials corresponds to the transfer of the anions $ZnTPPS^{4-}$ and tosylate from water to DCE.[24,26] The complex features observed at positive potentials are associated with the adsorption and transfer of $ZnTMPyP^{4+}$.[31,32] Specific adsorption of these porphyrin species appears to be linked to inhomogeneous solvation properties as a result of the hydrophilic groups in the meso position and the hydrophobic porphyrin ring. New evidences appear to show that porphyrins may undergo aggregation phenomena at the liquid/liquid boundary.[33] The solid line in Figure 2 depicts the polarizable window where no significant Faradaic responses are observed. For all subsequent experiments, the Galvani potential difference was constrained within these limits to avoid interferences from the porphyrin transfer in the photocurrent measurements. From the width of the polarizable window and the range of redox potentials

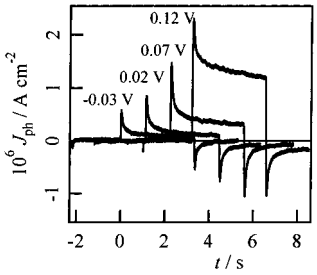

Figure 3. Photocurrent transient responses obtained in the presence of 10^{-3} mol dm^{-3} of ferrocene at various Galvani potential differences. The photon flux was 7.5×10^{16} s^{-1} cm^{-2} at 477 nm.

between Fc and $Me_{10}Fc$, it can be envisaged that the concentration-independent term of the electrochemical potential in the organic phase can be varied over a range close to 1 eV.

The photocurrent responses obtained in the presence of Fc as a function of the Galvani potential difference are illustrated in Figure 3. Monochromatic light at 477 nm with an incident photon flux of 7.5×10^{16} s^{-1} cm^{-2} was employed for these measurements. A clear feature in these results is the increase of the photocurrent magnitude with increasing applied potentials. The relaxation after the initial photocurrent and the overshoot upon interruption of the illumination indicate a back charge-transfer process.[24,27,34,35] Indeed, our previous studies have shown that reduced porphyrin species can reinject an electron back to the oxidized ferrocene unit prior to the final product separation. So far, we have treated the product-separation process as a dissociation step of an interfacial geminate ion pair. However, a more rigorous treatment should involve desorption dynamics and diffusion of photoproducts away from the interface. We are currently modeling these processes to have a quantitative expression for the displacement current.

It should also be considered that the photocurrent responses in Figure 3 could be affected by the transfer of photogenerated Fc^+ from the organic to the aqueous phase. The formal transfer potential of this ion is $\Delta_o^w \phi^{o\prime}_{Fc^+} = 0.005$ V $\pm$ 0.010 V;[1] therefore, the partitioning equilibrium will be displaced toward the aqueous phase at more negative potentials. Indeed, preliminary simulations of the concentration profiles of photoproducts at the interface indicate that the overall photocurrent can be decreased by a coupled ion-transfer process assuming rate constants above 10^{-2} cm s^{-1}. We shall discuss details of the simulations in a separate publication.[36] For the other ferrocene derivatives, the formal transfer potentials of the corresponding cation are more negative than $\Delta_o^w \phi^{o\prime}_{Fc^+}$, and the effects related to the transfer of photoproducts are negligible throughout the whole potential range. As discussed below, most of the data employed in our analysis were obtained under conditions where attenuation of the photocurrent due to the transfer of photoproducts is not significant.

The photocurrent transients can be rationalized in terms of two sets of competing reactions: (i) relaxation of the excited state vs heterogeneous electron transfer and (ii) product separation vs back charge transfer. The former competition involves an electron-transfer step to the triplet state of the porphyrin complex. Although a detailed photophysical description of this heterodimer is still in progress, previous studies by Linschitz and co-workers indicate that the lifetime of the triplet states of porphyrin dimers are similar to those of the monomers.[37−39] Based on preliminary pump−probe second harmonic generation studies of the ZnTMPyP porphyrin adsorbed at the water/DCE interface, a triplet state lifetime on the order of 5 μs was obtained.[40] Consequently, the average time associated with electron tunneling from Fc to the excited state of the porphyrin should take place in this time scale. The competition involving back charge transfer and product separation can be accessed by dynamic photoelectrochemical measurements such as intensity-modulated photocurrent spectroscopy.[25,27] The typical relaxation times associated with the photocurrent decay in Figure 3 are of the order of tens of milliseconds.

Taking into account the two sets of competing reactions, the steady-state photocurrent can be expressed as[25−27,34]

$$J_{ph}^{ss} = J_{ph}^{max}\left(\frac{k_{et}}{k_{et} + k_d}\right)\left(\frac{k_{ps}}{k_{ps} + k_{back}}\right) \qquad (6)$$

where k_{et} is the pseudo-first-order rate constant of electron transfer with respect to the excited state, k_d is the rate constant associated with the decay of the excited state, k_{back} and k_{ps} are the rate constants of back charge transfer and product separation, respectively. Because the electron transfer is in competition with the decay of the excited state, the dimension of k_{et} can be defined in terms of a pseudo-first-order quenching reaction (units of s^{-1}). This constant can be regarded as the inverse of the average transient time of electrons across the liquid/liquid boundary. In our phenomenological approach, the units of k_{ps} and k_{back} have also been taken as first order, s^{-1}.[25,27] The parameter J_{ph}^{max} corresponds to the photocurrent for an internal quantum yield of unity, that is, $k_{et} \gg k_d$ and $k_{ps} \gg k_{back}$. This parameter is proportional to the photon flux (I_0) and the surface excess of porphyrin (Γ_S),

$$J_{ph}^{max} = e\Gamma_S \sigma I_0 \qquad (7)$$

where σ is the optical capture cross section. Previous studies have shown that the coverage of the porphyrin heterodimer is close to a full monolayer for the concentrations indicated in Figure 1.[26] Taking 2.5×10^{14} cm^{-2} and 10^{-17} cm^2 for Γ_s and σ, respectively, the value of J_{ph}^{max} can be estimated to be 3×10^{-5} A cm^{-2} for a photon flux of 7.5×10^{16} s^{-1} cm^{-2} at 477 nm. This estimation allows prediction of the maximum conversion efficiency on the order of 0.2% at this wavelength.

For the subsequent analysis, it will be assumed that the initial photocurrent (J_{ph}^0) on the transient responses is determined by

$$J_{ph}^0 = J_{ph}^{max}\left(\frac{k_{et}}{k_{et} + k_d}\right) \qquad (8)$$

This assumption is based on the different time scales for the electron-transfer dynamics and the back charge-transfer response. As Γ_S is effectively independent of the Galvani potential difference, the potential dependence of J_{ph}^0 reflects the behavior of the ratio between k_{et} and k_d.

The photocurrent responses strongly increase as the redox potential of the electron donor becomes more negative. This trend can be clearly observed by comparing the photocurrent transients in Figure 4 and the data in Table 1. The transient responses in Figure 4a,b were obtained at 0 V and for the same photon flux as that indicated in Figure 3. In addition to the increase of the photocurrent responses, the back charge-transfer relaxation decreases as the redox potential decreases. For instance, the photocurrent transients in the presence of $Me_{10}Fc$ exhibit a quasi square wave response, reflecting the absence of back electron-transfer response. The dependence of the photocurrent and the back charge-transfer relaxation on the redox potential of the electron donor can be rationalized by the diagram in Figure 4c. As the redox potential of the donor becomes more

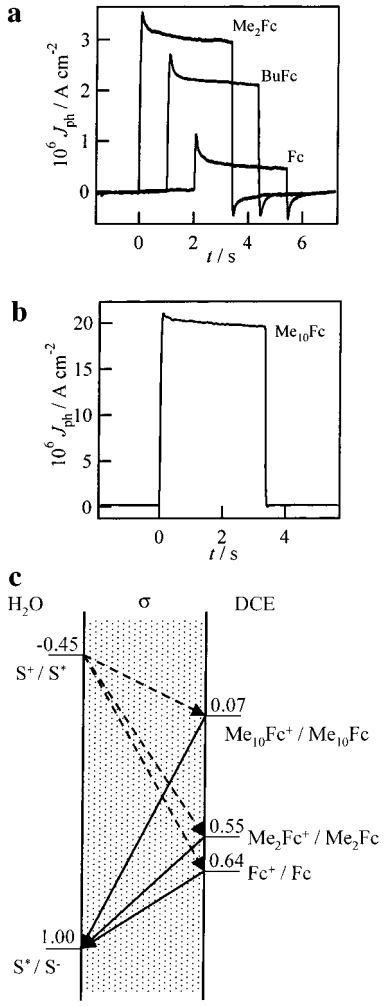

Figure 4. Photocurrent transient responses in the presence of 10^{-3} mol dm^{-3} of ferrocene, dimethylferrocene, butylferrocene (a), and decamethylferrocene (b) at $\Delta_o^w\phi = 0$ V. The diagram in panel c shows the redox potentials of the heterodimer triplet state and the redox quencher in the organic phase. The liquid/liquid boundary is denoted by σ. It is observed that the photocurrent increases and the back charge transfer decreases as the redox potential of the quencher becomes more negative. The full and dotted arrows link the redox couples involved in the photoinduced and back electron transfer, respectively.

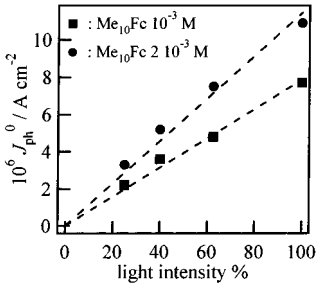

Figure 5. Initial photocurrent, J_{ph}^0, as function of the illumination intensity for two concentrations of decamethylferrocene in the organic phase. Illumination was provided by a 450 W arc-Xe lamp and modified by neutral density filters. The linear behavior indicates that diffusion effects are negligible in the present range of photocurrent density.

negative, the driving force for the photoinduced electron transfer increases, while that for the back charge transfer decreases.

The behavior of the photocurrent responses in the presence of $Me_{10}Fc$ at 0 V as a function of the light intensity is illustrated in Figure 5. The linear dependence observed is consistent with eq 7, indicating that the surface excess of the porphyrin can be

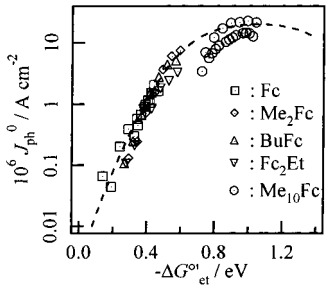

Figure 6. Photocurrent dependence on the formal Gibbs energy of electron transfer as estimated from eq 9. Dashed line corresponds to a fit of eq 12 to the experimental data, taking Z and λ as adjustable parameters.

taken as constant under the current illumination levels. This is also consistent with the square shape of the photocurrent transient shown in Figure 4b. This behavior indicates that diffusion effects involving not only the porphyrin excited state but also the redox couple in the organic phase are negligible.

From the energy diagram in Figure 4c, the difference in the Gibbs energy of electron transfer, also known as driving force, can be defined as

$$\Delta G_{et}^{\circ\prime} = -F([E_{S^*/S^-}^{\circ\prime,w}]_{SHE} - [E_{Q^+/Q}^{\circ\prime,DCE}]_{SHE} + \Delta_o^w\phi) \qquad (9)$$

where the values of $[E_{S^*/S^-}^{\circ\prime,w}]_{SHE}$ and $[E_{Q^+/Q}^{\circ\prime,DCE}]_{SHE}$ are summarized in Table 1. From the potential dependence of J_{ph}^0 observed for the various ferrocene derivatives, the photocurrent dependence on $\Delta G_{et}^{\circ\prime}$ can be estimated as shown in Figure 6. A rather interesting feature of these results is that the dependence of the photocurrent on $\Delta G_{et}^{\circ\prime}$ is considerably weaker for values close to -1 eV. According to eq 8, the behavior of the photocurrent at rather negative $\Delta G_{et}^{\circ\prime}$ may reflect that either $k_{et} \gg k_d$ under these conditions or the dependence of k_{et} on $\Delta G_{et}^{\circ\prime}$ becomes effectively weaker. However, the fact that the photocurrent increases upon doubling the concentration of $Me_{10}Fc$ as depicted in Figure 5 clearly indicates that the internal quantum yield is still smaller than one. Furthermore, the value of J_{ph}^0 remains smaller than that predicted for J_{ph}^{max}, suggesting that the behavior in Figure 6 is connected to a decrease in the dependence of the rate constant k_{et} on $\Delta G_{et}^{\circ\prime}$.

As we mentioned earlier, the possibility of Fc^+ transfer from DCE to the aqueous phase could attenuate the photocurrent density depending on the difference between $\Delta_o^w\phi_{Fc^+}^{\circ\prime}$ and $\Delta_o^w\phi$. According to our preliminary simulations,[36] the range in which this attenuation may be significant corresponds to $-\Delta G_{et}^{\circ} < 0.35$ eV. However, no clear changes in the dependence of J_{ph}^0 on $\Delta G_{et}^{\circ\prime}$ can be seen in this region that could indicate the presence of coupled ion transfer. Indeed, in the next section, we shall demonstrate that the results in Figure 6 can be interpreted in terms of the Marcus expression for nonadiabatic electron-transfer reaction.

3.2. Electron-Transfer Dynamics as a Function of the Gibbs Energy Difference. Within the framework of Marcus theory, the activation energy for a nonadiabatic electron-transfer process is given by[41−44]

$$\Delta G_{act} = w_r + \frac{(\lambda + \Delta G_{et}^{\circ\prime} + w_p - w_r)^2}{4\lambda} \approx \frac{(\lambda + \Delta G_{et}^{\circ\prime})^2}{4\lambda} \qquad (10)$$

where w_r and w_p are the work terms related to reactants encounter and product separation, which could be neglected as a first approximation. The reorganization energy, λ, involves contributions from internal conformation changes of the reac-

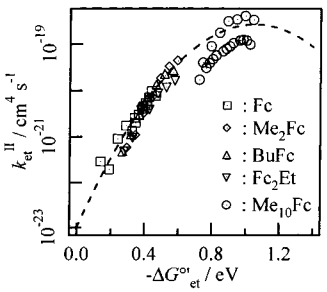

Figure 7. Bimolecular heterogeneous electron-transfer rate constant as a function of $\Delta G_{et}^{o\prime}$ as derived from the data in Figure 6. The estimated average distance $R = 0.8$ nm was employed for calculating k_{et}^{II} using eqs 11 and 13.

tants as well as solvation structure during the electron-transfer step. Assuming a sharp liquid/liquid boundary that cannot be penetrated by the reactants, the relationship between the activation energy and the bimolecular electron-transfer rate constant, k_{et}^{II} (units of cm^4 s^{-1}), corresponds to[41]

$$k_{et}^{II} = 2\pi\kappa\nu(a_S + a_Q)\Delta R^3 \exp(-\Delta G_{act}/(k_B T)) \qquad (11)$$

where κ is the Landau−Zener transmission coefficient, ν is the frequency of nuclear motion and ΔR is the characteristic distance where the volume integrand is maximized. The parameters a_S and a_Q correspond to the molecular radii of the sensitizer and the redox quencher. The dimensionality of the rate constants k_{et} and k_{et}^{II} should be clearly differentiated. The former corresponds to an average of the excited-state quenching rate constant, in which the characteristic tunnelling distance and the concentration of the redox quencher are included. On the other hand, k_{et}^{II} is independent of the quencher concentration and is defined for a given average distance between the redox species. Obviously, both parameters are closely related as discussed further below. From eqs 8, 10, and 11, the photocurrent responses can be expressed as

$$J_{ph}^0 = J_{ph}^{max} \frac{\exp(-(\lambda + \Delta G_{et}^{o\prime})^2/(4\lambda k_B T))}{\exp(-(\lambda + \Delta G_{et}^{o\prime})^2/(4\lambda k_B T)) + k_d/Z} \qquad (12)$$

where Z corresponds to the maximum value of the electron-transfer rate constant expressed in units of a homogeneous pseudo-first-order reaction with respect to the concentration of the excited state. This parameter is determined by the preexponential term in eq 11, the characteristic distance separating the redox species at the interface (R), and the concentration of the quencher (c_Q):

$$Z = \frac{2\pi\kappa\nu(a_S + a_Q)(\Delta R^3)N_A c_Q}{R} \qquad (13)$$

The ratio k_d/Z as well as λ were evaluated from nonlinear least-square fitting of eq 12 to the curve in Figure 6, taking $J_{ph}^{max} = 3 \times 10^{-5}$ A cm^{-2}. The dashed line in Figure 6 was obtained for $k_d/Z = 0.5$ and a reorganization energy $\lambda = 1.05 \pm 0.05$ eV. The former value confirms that the characteristic transient time of the electron transfer is of the same order of magnitude as the decay of the excited state.[26,27,34] On the other hand, the reorganization energy appears somewhat larger than previous estimations based on SECM measurements at nonpolarizable interfaces.[22,23] To rationalize the origin of λ, the photoelectrochemical behavior of this system can be compared to the charge-transfer dynamics at porphyrin−ferrocene dyads. Imahori et al. have shown that the quenching of zinc tetraphenylporphyrin−ferrocene dyads takes place via the single state with a rate constant in the range of 10^8 s^{-1}.[45,46] As discussed later, this rate constant is 2−3 orders of magnitude larger than the values estimated for ferrocene. Consequently, the large value of λ appears to be connected to solvent reorganization rather than changes in the internal conformation of the redox species.

Considering an impenetrable sharp liquid/liquid boundary, the solvent reorganization energy can be expressed as[41,47,48]

$$\lambda_s = \frac{(\Delta e)^2}{4\pi\epsilon_0}\left(\frac{1}{\epsilon_o^{op}} - \frac{1}{\epsilon_o^{s}}\right)\left(\frac{1}{2a_Q}\right) + \frac{(\Delta e)^2}{4\pi\epsilon_0}\left(\frac{1}{\epsilon_w^{op}} - \frac{1}{\epsilon_w^{s}}\right)\left(\frac{1}{2a_S}\right) + \frac{(\Delta e)^2}{4\pi\epsilon_0}\left(\frac{1}{4d_o}\right)\left(\frac{\epsilon_o^{op} - \epsilon_w^{op}}{\epsilon_o^{op}(\epsilon_o^{op} + \epsilon_w^{op})} - \frac{\epsilon_o^{s} - \epsilon_w^{s}}{\epsilon_o^{s}(\epsilon_o^{s} + \epsilon_w^{s})}\right) + \frac{(\Delta e)^2}{4\pi\epsilon_0}\left(\frac{1}{4d_w}\right)\left(\frac{\epsilon_w^{op} - \epsilon_o^{op}}{\epsilon_w^{op}(\epsilon_w^{op} + \epsilon_o^{op})} - \frac{\epsilon_w^{s} - \epsilon_o^{s}}{\epsilon_w^{s}(\epsilon_w^{s} + \epsilon_o^{s})}\right) - \frac{(\Delta e)^2}{4\pi\epsilon_0}\left(\frac{2}{R}\right)\left(\frac{1}{\epsilon_o^{op} + \epsilon_w^{op}} - \frac{1}{\epsilon_o^{s} + \epsilon_w^{s}}\right) \qquad (14)$$

where d_o and d_w are the characteristic distances between the interface boundary and the center of the reactive species. Taking the various parameters in eq 14 as $a_Q \approx 0.2$ nm, $a_S \approx 0.7$ nm, $d_o = d_w = R/2$, $\epsilon_w^{op} = 1.78$, $\epsilon_o^{op} = 2.09$, $\epsilon_w^{s} = 78.4$ and $\epsilon_o^{s} = 10$, the estimated solvent reorganization energy of 1.05 eV corresponds to an average distance R of 0.8 nm.

The value of R is comparable to the solvent profile distribution obtained from molecular dynamic simulations,[3,4] as well as spectroscopic techniques.[5,6] However, it should be considered that our analysis is based on the sharp liquid/liquid boundary assumption, in which the dielectric properties of the interface are described by a step function. A more complex analysis will be required to account for progressive changes in permittivity, although we believe that the main conclusions derived from the present approach will remain unaffected.

Providing a value for the rate constant of the excited-state decay, the dependence of k_{et}^{II} on $\Delta G_{et}^{o\prime}$ can be reconstructed from the data in Figure 6 and eqs 11−13. However, the absolute value obtained from this analysis should be taken cautiously because of uncertainties in the value of k_d for the porphyrin heterodimer. On the basis of time-resolved EPR[39] and second harmonic generation,[40] we shall consider k_d on the order of 10^6 s^{-1}. The behavior in Figure 7 shows that, despite the rather negative values of Gibbs energy of electron transfer, the inverted Marcus region is yet to be attained. Recent measurements employing other metallocenes with more negative redox potentials, for example, titanocene dichloride, appear to show a decrease in the bimolecular electron-transfer rate constant. However, the trends obtained were obscured by the high instability of these species. The maximum value for k_{et}^{II} is approximately 3×10^{-19} cm^4 s^{-1}, which is consistent with the nonadiabatic limit calculated by Smith et al.[49] In this work, the distance dependence of the Landau−Zener transmission coefficient was included in the spatial integration leading to the macroscopic electron-transfer rate constant. In the original work by Marcus,[41] the transmission coefficient was not included in the overall integrand, which may lead to underestimation of the rate constant for systems with large electronic coupling. However, our estimations of k_{et}^{II} do reveal a rather low degree of electronic coupling, validating Marcus' approximations. This nonadiabatic character of the heterogeneous quenching of the

porphyrins is associated with the distance separating the redox species at the interface.

4. Conclusions

Photocurrent responses originating from the heterogeneous quenching of the heterodimer ZnTPPS−ZnTMPyP by ferrocene derivatives exhibit a well-defined dependence on $\Delta G_{et}^{\circ\prime}$. The driving force for the photoinduced electron transfer was modified via tuning the Galvani potential difference across the interface as well as by employing a series of ferrocene derivatives with different redox potentials. The photocurrent dependence on $\Delta G_{et}^{\circ\prime}$ was rationalized in terms of a Marcus-type behavior of the phenomenological electron-transfer rate constant, providing a reorganization energy of 1.05 ± 0.05 eV. Considering the substantially faster electron-transfer dynamics between porphyrins and ferrocene in homogeneous phase,[45,46] the value of λ appears to be determined by the solvent reorganization term. Within the framework of Marcus' model for sharp liquid/liquid boundary, the magnitude of λ_s allowed calculation of an average distance between the redox species of 0.8 nm. Furthermore, the activation-less limit of the bimolecular electron-transfer rate constant was estimated to be 3×10^{-19} cm^4 s^{-1}. All of these parameters appear to indicate a strong nonadiabatic character of the electron-transfer process arising from the apparent average distance between the redox species.

Finally, the clear dependence of k_{et}^{II} on the Galvani potential difference has some important implications on our current understanding of the potential distribution across the interface. These results indicate that a substantial portion of the Galvani potential difference is developed within the average distance between the redox species, that is, 0.8 nm. This potential distribution is substantially sharper than that estimated from simplified approximations based on the Poisson−Boltzmann distribution.[50] To further address this issue, an essential parameter to control is the distance separating the redox species. This could be achieved by designing porphyrin dyads featuring rigid spacers with self-assembling properties at the liquid/liquid interface. By analyzing the effect of the spacer length on the magnitude of the electron-transfer rate constant and on the potential dependence, we expect to probe the potential distribution across the interface.

Acknowledgment. We are grateful to Professor R. A. Marcus and to Dr. Henrik Jensen for the fruitful discussions. The technical assistance by Valerie Devaud is also acknowledged. This work has been supported by the Fonds National Suisse de la Recherche Scientifique (Grant 20-055692.98/1).

References and Notes

(1) Fermín, D. J.; Lahtinen, R. In *Liquid interfaces in chemical, biological and pharmaceutical applications*; Volkov, A. G., Ed.; Marcel Dekker Inc.: Boca Raton, FL, 2001; pp 179−228.
(2) Amemiya, S.; Ding, Z. F.; Zhou, J. F.; Bard, A. J. *J. Electroanal. Chem.* **2000**, *483*, 7−17.
(3) Benjamin, I. *Annu. Rev. Phys. Chem.* **1997**, *48*, 407.
(4) Benjamin, I. *Chem. Rev.* **1996**, *96*, 1449−1475.
(5) Strutwolf, J.; Barker, A. L.; Gonsalves, M.; Caruana, D. J.; Unwin, P. R.; Williams, D. E.; Webster, J. R. P. *J. Electroanal. Chem.* **2000**, *483*, 163−173.
(6) Webster, R. D.; Beaglehole, D. *Phys. Chem. Chem. Phys.* **2000**, *2*, 5660−5666.
(7) Frank, S.; Schmickler, W. *J. Electroanal. Chem.* **2000**, *483*, 18−21.
(8) Frank, S.; Schmickler, W. *J. Electroanal. Chem.* **2001**, *500*, 491−497.
(9) Schmickler, W. *J. Electroanal. Chem.* **1997**, *428*, 123−127.
(10) Pereira, C. M.; Schmickler, W.; Silva, F.; Sousa, M. J. *J. Electroanal. Chem.* **1997**, *436*, 9−15.
(11) Tsionsky, M.; Bard, A. J.; Mirkin, M. V. *J. Phys. Chem.* **1996**, *100*, 17881−17888.
(12) Tsionsky, M.; Bard, A. J.; Mirkin, M. V. *J. Am. Chem. Soc.* **1997**, *119*, 10785−10792.
(13) Barker, A. L.; Unwin, P. R.; Zhang, J. *Electrochem. Commun*. **2001**, *3*, 372−378.
(14) Zhang, J.; Barker, A. L.; Unwin, P. R. *J. Electroanal. Chem.* **2000**, *483*, 95−107.
(15) Zhang, J.; Unwin, P. R. *J. Phys. Chem. B* **2000**, *104*, 2341−2347.
(16) Liu, B.; Mirkin, M. V. *J. Am. Chem. Soc.* **1999**, *121*, 8352−8355.
(17) Shi, C. N.; Anson, F. C. *J. Phys. Chem. B* **1999**, *103*, 6283−6289.
(18) Shi, C. N.; Anson, F. C. *J. Phys. Chem. B* **1998**, *102*, 9850−9854.
(19) Shi, C. N.; Anson, F. C. *J. Phys. Chem. B* **2001**, *105*, 8963−8969.
(20) Ding, Z.; Fermín, D. J.; Brevet, P.-F.; Girault, H. H. *J. Electroanal. Chem.* **1998**, *458*, 139−148.
(21) Zu, Y. B.; Fan, F. R. F.; Bard, A. J. *J. Phys. Chem. B* **1999**, *103*, 6272−6276.
(22) Barker, A. L.; Unwin, P. R.; Amemiya, S.; Zhou, J. F.; Bard, A. J. *J. Phys. Chem. B* **1999**, *103*, 7260−7269.
(23) Ding, Z. F.; Quinn, B. M.; Bard, A. J. *J. Phys. Chem. B* **2001**, *105*, 6367−6374.
(24) Fermín, D. J.; Doung, H.; Ding, Z.; Brevet, P.-F.; Girault, H. H. *Electrochem. Commun*. **1999**, *1*, 29−32.
(25) Lahtinen, R.; Fermín, D. J.; Kontturi, K.; Girault, H. H. *J. Electroanal. Chem.* **2000**, *483*, 81−87.
(26) Fermín, D. J.; Duong, H.; Ding, Z.; Brevet, P.-F.; Girault, H. H. *J. Am. Chem. Soc.* **1999**, *121*, 10203−10210.
(27) Fermín, D. J.; Duong, H.; Ding, Z.; Brevet, P.-F.; Girault, H. H. *Phys. Chem. Chem. Phys.* **1999**, *1*, 1461−1467.
(28) See the web site dcwww.epfl.ch for a comprehensive list of free energy of ion transfer at various liquid/liquid interfaces.
(29) Kalyanasundaram, K.; Neumann-Spallart, M. *J. Phys. Chem.* **1982**, *86*, 5163−5169.
(30) Kalyanasundaram, K. *Photochemistry of Polypyridine and Porphyrin Complexes*; Academic Press: London, 1992.
(31) Nagatani, H.; Fermín, D. J.; Girault, H. H. *J. Phys. Chem. B* **2001**, *105*, 9463−9473.
(32) Nagatani, H.; Iglesias, R. A.; Fermín, D. J.; Brevet, P. F.; Girault, H. H. *J. Phys. Chem. B* **2000**, *104*, 6869−6876.
(33) Nagatani, H.; Piron, A.; Brevet, P.-F.; Fermín, D. J.; Girault, H. H. *Langmuir*, submitted for publication.
(34) Fermín, D. J.; Ding, Z.; Duong, H.; Brevet, P.-F.; Girault, H. H. *J. Phys. Chem. B* **1998**, *102*, 10334−10341.
(35) Fermín, D. J.; Ding, Z.; Duong, H. D.; Brevet, P. F.; Girault, H. H. *J. Chem. Soc., Chem. Commun.* **1998**, 1125−1126.
(36) Samec, Z.; Eugster, N.; Fermín, D. J.; Girault, H. H., manuscript in preparation.
(37) van Willigen, H.; Das, U.; Ojadi, E.; Linschitz, H. *J. Am. Chem. Soc.* **1985**, *107*, 7784−7785.
(38) Ojadi, E.; Selzer, R.; Linschitz, H. *J. Am. Chem. Soc.* **1985**, *107*, 7783−7784.
(39) Hugerat, M.; Levanon, H.; Ojadi, E.; Biczok, L.; Linschitz, H. *Chem. Phys. Lett.* **1991**, *181*, 400−406.
(40) Piron, A. Ph.D. Thesis, Ecole Polytechnique Fédérale de Lausanne, Lausanne, Switzerland, 2001.
(41) Marcus, R. A. *J. Phys. Chem.* **1990**, *94*, 4152−4155.
(42) Marcus, R. A. *J. Phys. Chem.* **1990**, *94*, 7742.
(43) Marcus, R. A. *J. Phys. Chem.* **1990**, *94*, 1050−1055.
(44) Marcus, R. A. *J. Phys. Chem.* **1991**, *95*, 2010−2013.
(45) Imahori, H.; Yamada, H.; Nishimura, Y.; Yamazaki, I.; Sakata, Y. *J. Phys. Chem. B* **2000**, *104*, 2099−2108.
(46) Imahori, H.; Tamaki, K.; Guldi, D. M.; Luo, C. P.; Fujitsuka, M.; Ito, O.; Sakata, Y.; Fukuzumi, S. *J. Am. Chem. Soc.* **2001**, *123*, 2607−2617.
(47) Girault, H. H. *J. Electroanal. Chem.* **1995**, *388*, 93−100.
(48) Benjamin, I.; Kharkats, Y. I. *Electrochim. Acta* **1998**, *44*, 133−138.
(49) Smith, B. B.; Halley, J. W.; Nozik, A. J. *Chem. Phys.* **1996**, *205*, 245−267.
(50) Samec, Z. *Chem. Rev.* **1988**, *88*, 617−632.